

# Single-shot Kramers–Kronig complex orbital angular momentum spectrum retrieval

Zhongzheng Lin,<sup>a,†</sup> Jianqi Hu<sup>Ⓜ,b,\*†</sup> Yujie Chen,<sup>a</sup> Camille-Sophie Brès<sup>Ⓜ,b</sup> and Siyuan Yu<sup>a,\*</sup>

<sup>a</sup>Sun Yat-sen University, School of Electronics and Information Technology, State Key Laboratory of Optoelectronic Materials and Technologies, Guangzhou, China

<sup>b</sup>École Polytechnique Fédérale de Lausanne, Photonic Systems Laboratory, STI-IEM, Lausanne, Switzerland

**Abstract.** Orbital angular momentum (OAM) spectrum diagnosis is a fundamental building block for diverse OAM-based systems. Among others, the simple on-axis interferometric measurement can retrieve the amplitude and phase information of complex OAM spectra in a few shots. Yet, its single-shot retrieval remains elusive, due to the signal–signal beat interference inherent in the measurement. Here, we introduce the concept of Kramers–Kronig (KK) receiver in coherent communications to the OAM domain, enabling rigorous, single-shot OAM spectrum measurement. We explain in detail the working principle and the requirement of the KK method and then apply the technique to precisely measure various characteristic OAM states. In addition, we discuss the effects of the carrier-to-signal power ratio and the number of sampling points essential for rigorous retrieval and evaluate the performance on a large set of random OAM spectra and high-dimensional spaces. Single-shot KK interferometry shows enormous potential for characterizing complex OAM states in real time.

**Keywords:** orbital angular momentum; Kramers–Kronig relations; single-shot measurement; phase retrieval.

Received Mar. 12, 2023; revised manuscript received Apr. 26, 2023; accepted for publication May 19, 2023; published online Jun. 12, 2023.

© The Authors. Published by SPIE and CLP under a Creative Commons Attribution 4.0 International License. Distribution or reproduction of this work in whole or in part requires full attribution of the original publication, including its DOI.

[DOI: [10.1117/1.AP.5.3.036006](https://doi.org/10.1117/1.AP.5.3.036006)]

## 1 Introduction

Structured light waves with spiral phase fronts carry orbital angular momentum (OAM). Such helical optical beams, either naturally emitted from laser cavities<sup>1</sup> or externally sculpted,<sup>2</sup> have recently attracted significant attention and have been widely used in communication, sensing, imaging, as well as classical and quantum information processing.<sup>3–7</sup> For many of these applications, the ability to diagnose an arbitrary OAM state is essential, so its complex structure can be unveiled and decomposed into an orthogonal OAM basis. Various methods have been explored for the task. Perhaps the most straightforward approach is using vortex phase plates together with a mode filter to obtain the power of each OAM order sequentially.<sup>2,8</sup> The number of measurements required by this approach, however, scales fast with the measurement space. Techniques based on

the far-field diffraction patterns through certain types of apertures<sup>9</sup> or gratings<sup>10,11</sup> generally only identify pure OAM orders rather than superimposed states. In that sense, mode sorters are efficient in separating the superposition of OAM modes by mapping different OAM orders into different spatial positions. They have been implemented based on cascaded Mach–Zehnder interferometers with Dove prisms,<sup>12</sup> log-polar transformation,<sup>13,14</sup> and its improvement by means of beam copying,<sup>15</sup> or spiral transformation<sup>16</sup> that increases the mode separation. Moreover, multi-plane light conversion is also employed for sorting OAM modes with enhanced functionalities.<sup>17–19</sup> Yet, mode sorters generally lose the relative phase information among OAM modes, which may be required in many scenarios to unambiguously reconstruct the complex OAM states. For this purpose, the interference measurement techniques are appealing for OAM full-field (amplitude and phase) retrieval.<sup>20–24</sup>

Typical OAM interference measurements are performed by recording the interferograms of a complex signal field and a reference OAM mode (or Gaussian beam) with a camera.<sup>21–23</sup> Since the camera records the light intensity, the complex signal

\*Address all correspondence to Jianqi Hu, [jianqi.hu@epfl.ch](mailto:jianqi.hu@epfl.ch); Siyuan Yu, [yusy@mail.sysu.edu.cn](mailto:yusy@mail.sysu.edu.cn)

<sup>†</sup>The authors contributed equally to this work.

field cannot be directly retrieved from the intensity-only measurement. The measured interferogram intensity, however, consists of not only the desired interference between the signal and reference beams but also the self-beating of both of them. While the power of the reference is constant across the azimuthal angle, the existence of the signal–signal beat interference (SSBI) complicates the signal retrieval process. Multiple interferograms are thus required to remove the SSBI by adjusting the power<sup>21,22</sup> and/or phase<sup>23</sup> of the reference light. Single-shot interferometric measurement has been demonstrated in the context of partially coherent fields, but only for symmetric OAM spectra, while two shots are still needed for generalized spectral shapes.<sup>24</sup> Although the SSBI contribution may be omitted when the reference beam is sufficiently strong,<sup>21</sup> rigorous, single-shot retrieval remains elusive for conventional on-axis interferometry.

Notably, the interference measurement of the complex OAM spectrum resembles the detection of complex modulated signals in coherent optical communications, where the reference beam is the counterpart of the local oscillator. A phase-diverse coherent receiver is generally used to retrieve both the amplitude and phase of the modulated signal.<sup>25</sup> In recent years, considerable efforts have been made to reduce the receiver complexity in coherent communication systems, ideally by using only one single-ended photodetector.<sup>26–31</sup> The Kramers–Kronig (KK) receiver is an effective solution for direct detection of complex-valued signals.<sup>28–31</sup> In this case, the receiver works in a heterodyne scheme and requires that the frequency of the local oscillator be outside the signal’s spectrum. When the interference waveform satisfies the minimum-phase condition,<sup>31</sup> the signal can be rigorously reconstructed from the intensity measurement via the KK relation. This greatly simplifies the receiver architecture into the straightforward direct detection. In addition, similar KK-based full-field retrieval has also been applied for holographic imaging exploring the space–time duality.<sup>32,33</sup>

In this work, by drawing a close analogy between the time-frequency and azimuth–OAM domains, we extend the KK retrieval concept into the OAM space, for the first time to our knowledge. Such an approach enables the readout of both the amplitude and phase relation of an arbitrary OAM state in a single-shot manner without increasing the system complexity. We describe in detail the retrieval procedure, which is experimentally validated in a high-dimensional OAM space. In particular, we demonstrate the diagnosis of a number of characteristic OAM states,<sup>34–37</sup> including fractional OAM modes<sup>38</sup> that slightly violate the KK retrieval criteria. The typical parameters essential for a KK receiver,<sup>31</sup> i.e., the carrier-to-signal power ratio (CSPR) and the number of sampling points, are discussed in the context of OAM fields. Furthermore, we compare the performance of the proposed KK approach and the conventional Fourier approach for a large set of arbitrary OAM states, where the superiority of the KK approach is clearly shown. The single-shot nature of the KK method may find useful applications for characterizing OAM-based systems in real time.

## 2 Results

### 2.1 Principle of Operation

A complex OAM field can be described by the controlled superposition in discrete OAM mode basis.<sup>34</sup>

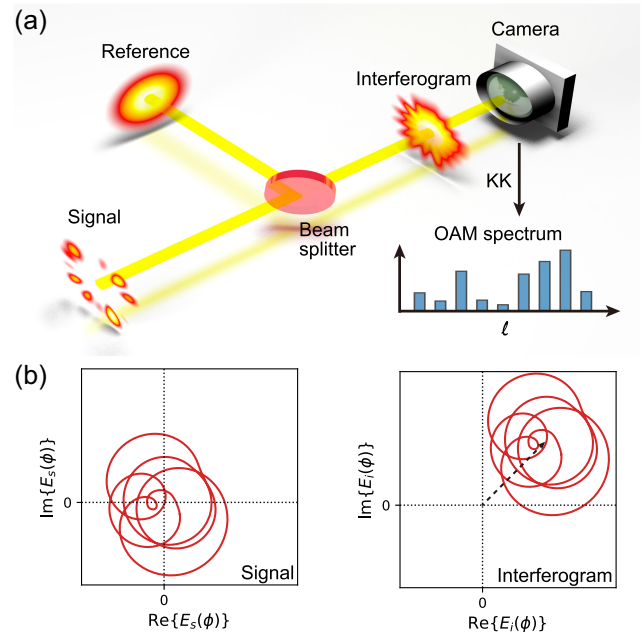


**Fig. 1** Conceptual setup and the requirement for the KK retrieval. (a) The signal field with a complex OAM spectrum is co-axially combined with a reference Gaussian beam. The intensity of their interferogram is recorded with a camera and is used for the spectrum retrieval. (b) The azimuthal trajectories of the signal (left) and the interferogram (right) in the complex plane. In order to meet the minimum phase condition, the trajectory must not encircle the origin. With the addition of a sufficiently large reference field (denoted by the dashed arrow), the interferogram satisfies the requirement, and thus the KK method can rigorously reconstruct the complex signal OAM spectrum.

$$E_s(\phi) = \sum_{l=l_0+1}^{l_0+N} a_l e^{il\phi + i\theta_l}, \quad (1)$$

where  $\phi$  is the azimuthal angle;  $a_l$  and  $\theta_l$  are the amplitude and phase of the  $l$ th OAM mode, respectively. Here, we consider the modal decomposition of the OAM field in the interval of  $[l_0 + 1, l_0 + N]$ , spanning an  $N$ -dimensional space. Without loss of generality, we assume  $l_0 = 0$  hereafter, as we can always use a phase mask with helical phase  $e^{-il_0\phi}$  to shift the OAM spectrum entirely above the zeroth order. In this study, the OAM fields are constructed based on perfect vortex modes<sup>39</sup> with identical radial distributions (see Note 1 in the [Supplemental Material](#)), such that we are only interested in field extraction in the azimuthal angle. As shown in Fig. 1(a), the complex signal field interferes with a reference beam with plane wave front  $E_r(\phi) = Ae^{i\theta_r}$ , where  $A$  is the amplitude of the reference mode, and  $\theta_r$  is the relative phase between the reference and signal fields. The CSPR value is defined as the ratio between the power of reference and signal beams averaged in the azimuthal angle, i.e.,  $\text{CSPR} = 10 \log \frac{\langle |E_r(\phi)|^2 \rangle}{\langle |E_s(\phi)|^2 \rangle}$ . Similar to the single-sideband modulation for a KK receiver in communications,<sup>28</sup> no guard band is needed in between the reference and the signal OAM spectra. Then, the interferogram is imaged with a camera, and its intensity in the azimuthal angle is proportional to

$$\begin{aligned}
 |E_i(\phi)|^2 &= |E_s(\phi) + E_r(\phi)|^2 \\
 &= A^2 + |E_s(\phi)|^2 + 2A \operatorname{Re}\{E_s(\phi)e^{-i\theta_r}\} \\
 &= A^2 + \left| \sum_{l=1}^N a_l e^{i\phi + i\theta_l} \right|^2 + 2A \sum_{l=1}^N a_l \cos(l\phi + \theta_l - \theta_r).
 \end{aligned} \quad (2)$$

The third term in the last equality of Eq. (2) contains all the Fourier coefficients  $a_l e^{i\theta_l}$  required to reconstruct the signal field, apart from scaling and a constant phase shift, while the second term corresponds to the SSBI.

To extract the phase information from a single intensity measurement, the amplitude and phase of the interferogram  $E_i(\phi)$  must be uniquely linked. A way to look at this is using the  $Z$ -extension as formulated in Ref. 31. By replacing the  $e^{i\phi}$  in  $E_i(\phi)$  with a variable  $Z$ , the interferogram becomes a polynomial function,

$$\mathcal{Z}_{E_i}(Z) = A e^{i\theta_r} + \sum_{l=1}^N a_l e^{i\theta_l} Z^l = \frac{A e^{i\theta_r}}{\prod_{l=1}^N (-z_l)} \prod_{l=1}^N (Z - z_l), \quad (3)$$

where  $z_l$  ( $l = 1, 2, \dots, N$ ) are the roots of  $\mathcal{Z}_{E_i}(Z) = 0$ , when  $a_N \neq 0$ . The second equality of Eq. (3) shows that  $\mathcal{Z}_{E_i}(Z)$  can be equivalently described by its zeros. Since the interferogram is under square-law detection, the zeros of  $|E_i(\phi)|^2$  are found using properties of  $Z$ -extension,<sup>31</sup>

$$\begin{aligned}
 \mathcal{Z}_{|E_i|^2}(Z) &= \mathcal{Z}_{E_i}(Z) \mathcal{Z}_{E_i^*}(Z) \\
 &= \frac{|A|^2}{Z^N \prod_{l=1}^N (-z_l)} \prod_{l=1}^N (Z - z_l) \left( Z - \frac{1}{z_l^*} \right),
 \end{aligned} \quad (4)$$

where  $*$  represents the complex conjugate. In Eq. (4), we obtain the zeros of  $\mathcal{Z}_{E_i^*}(Z)$  by conjugating Eq. (3).<sup>31</sup> As such, the zeros of  $\mathcal{Z}_{|E_i|^2}(Z)$  are in  $N$  pairs, comprising the zeros of  $\mathcal{Z}_{E_i}(Z)$  and the inverse of their complex conjugates. It is noted that replacing the zeros of  $\mathcal{Z}_{E_i}(Z)$  with their inverse conjugates would not modify the function  $\mathcal{Z}_{|E_i|^2}(Z)$ . This implies multiple different interferograms are mapped to the same intensity profile, thus causing ambiguity for the retrieval. If the interferogram is constructed such that all its zeros are outside or on the unit circle, also known as the minimum phase waveform,<sup>31</sup> one-to-one mapping between  $\mathcal{Z}_{E_i}(Z)$  and  $\mathcal{Z}_{|E_i|^2}(Z)$  is established. Evidently, a necessary and sufficient condition to be of a minimum phase waveform is that its trajectory does not encircle the origin of the complex plane.<sup>40</sup> This is visualized in Fig. 1(b). The left panel illustrates the azimuthal trajectory of a general OAM signal field  $E_s(\phi)$ , which does not meet the minimum phase requirement. With a sufficiently large reference field  $A e^{i\theta_r}$  (indicated by the dashed arrow), the azimuthal trajectory can be translated to match the minimum phase condition, as shown in the right panel of Fig. 1(b). Consequently, the amplitude and phase of the interferogram  $E_i(\phi)$  are uniquely related. It is worth mentioning that, for a given signal OAM field, the required reference intensity for the minimum phase condition varies with the relative angle  $\theta_r$ . Nevertheless, since no prior knowledge of the signal field is known, the reference amplitude needs to be greater than the signal's peak amplitude in the azimuthal angle, i.e.,  $A > |E_s(\phi)|$  for  $\phi \in [0, 2\pi)$ , thereby not encircling the

origin. With this we can calculate the minimum CSPR required for rigorous retrieval, which is set by the peak-to-average power ratio of the signal field.

Once the minimum phase condition is reached, for an interference field  $E_i(\phi) = |E_i(\phi)| e^{i \arg(E_i(\phi))}$  ( $\arg$  denotes the argument), the logarithm of its amplitude  $\log(|E_i(\phi)|)$  and phase  $\arg(E_i(\phi))$  are related by the Hilbert transform,<sup>31</sup>

$$\arg(E_i(\phi)) = \frac{1}{2\pi} p.v. \int_0^{2\pi} \cot\left(\frac{\phi - \phi'}{2}\right) \log(|E_i(\phi')|) d\phi', \quad (5)$$

where  $p.v.$  is the principal value. Note that due to the periodic nature of the azimuthal space, the kernel here in the Hilbert transform is in the cotangent form rather than the inverse, and the integration is over one circle.<sup>41</sup> From Eq. (5), we can reconstruct the full field of the interferogram  $E_i(\phi)$ , and thus also the signal full field  $E_s(\phi)$  by removing the constant reference term. Based on the Fourier relation, this equivalently gives the amplitude and phase of the OAM spectrum of  $E_s(\phi)$ .

## 2.2 Experimental KK Retrieval Procedure

In the experiment, the complex signal OAM fields are synthesized using computer-generated holograms and an optical 4-f system.<sup>42</sup> They consist of arbitrary superpositions of ring-shaped OAM modes with topological charges spanning 1 to 20. The OAM fields under test are then co-axially combined with a reference Gaussian beam, and their interferograms are recorded with a camera. The detailed experimental setup is described in the Note S1 in the [Supplemental Material](#). To satisfy the minimum phase condition, we tune the reference light power slightly above the power threshold set by the minimum required CSPR. Due to the signal preparation method we used,<sup>42</sup> the experimental and minimum required CSPR difference is kept constant ( $\sim 1$  dB) for different measurement instances (see Note S2 in the [Supplemental Material](#)). In the following, we demonstrate the KK retrieval procedure on a random complex OAM spectrum as an example. The top panel of Fig. 2(a) shows the measured camera images of the reference and the interference beams. Their azimuthal intensity distributions are extracted by sampling around the interfering regions (indicated by the dashed circles) and unwrapped as shown in the bottom panel of Fig. 2(a). It can be seen that the measured reference  $|E_r(\phi)|^2$  shows small intensity fluctuations in the azimuthal direction. Such a reference intensity pattern is unchanged while characterizing different signal OAM fields, so only their interferogram  $|E_i(\phi)|^2$  needs to be measured each time, suggesting that the retrieval process is a single shot.

Similar to the KK full-field retrieval in space and time,<sup>28,32</sup> digital upsampling may also be required in our case if the number of physical sampling points is not sufficiently large to cover the spectrum expended by the logarithmic operation.<sup>31</sup> The effect of upsampling is discussed in Note S3 in the [Supplemental Material](#). Throughout the paper, we take 71 azimuthal sampling points in the experiment, and then we digitally upsample the normalized interferogram  $|E_i(\phi)|^2/|E_r(\phi)|^2$  by 11 times for the subsequent processing. The top panel of the Fig. 2(b) shows the logarithm of the upsampled interferogram  $\log(|E_i(\phi)|/|E_r(\phi)|)$  as well as its Hilbert transform  $\arg(E_i(\phi)/E_r(\phi))$ . Instead of taking the convolution as defined in Eq. (5), the actual implementation of the Hilbert transform is



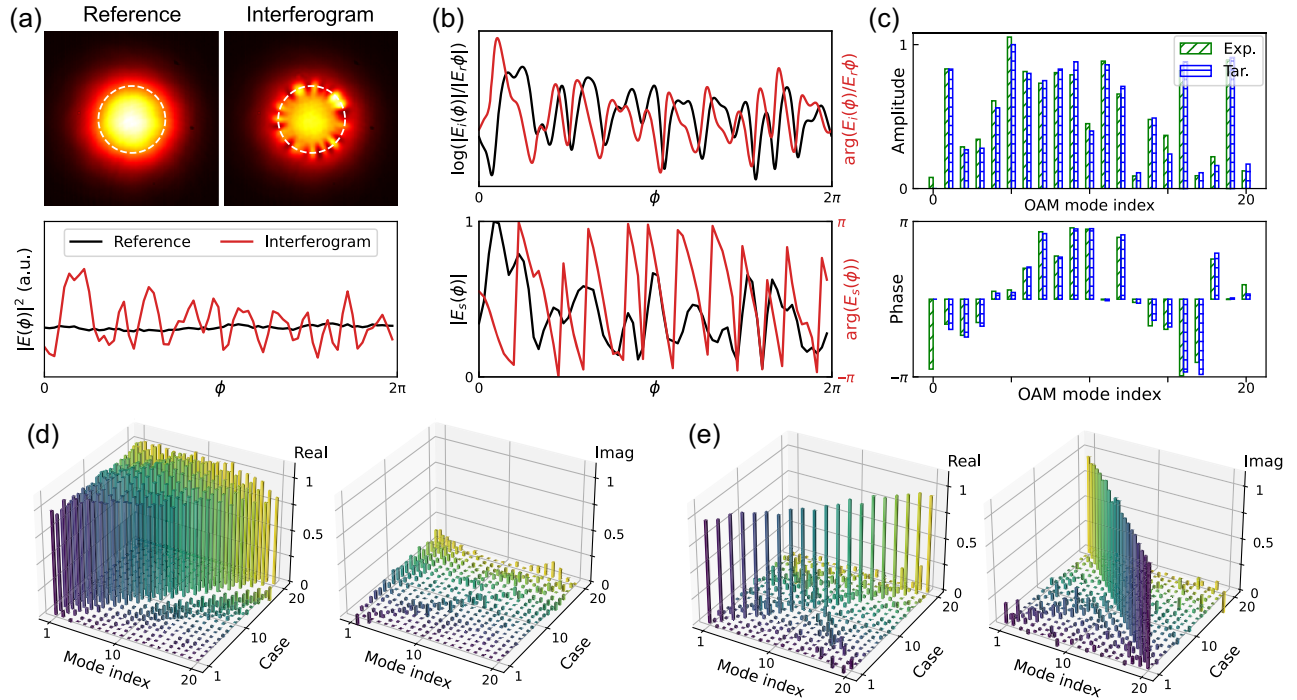


**Fig. 2** Experimental single-shot KK retrieval. (a)–(c) Retrieval process of an arbitrary OAM spectrum. (a) The intensity images of the reference (top left) and the interferogram (top right) are captured by a camera. By sampling along the dashed circles in the images, their azimuthal distributions are extracted (bottom). (b) The interferogram is then normalized and digitally up-sampled, whose phase is extracted from the Hilbert transform of the logarithm of its amplitude (top). From the full field of the interferogram, the amplitude and phase of the signal are obtained and downsampled to the original sampling points (bottom). (c) Taking the Fourier transform of the signal field derives the normalized amplitude (top) and relative phase relation (bottom) of the OAM spectrum. An accuracy of 97.6% is achieved by comparing the retrieved and the target OAM spectra. (d), (e) Measured 2D bar charts of the OAM states for (d) the superpositions of mode indices from 1 to  $n$  ( $n = 1, 2, \dots, 20$ ) with equal amplitudes and in-phase relations; (e) the superpositions of mode indices  $n$  and  $21 - n$  ( $n = 1, 2, \dots, 20$ ) with equal amplitudes and a  $\pi/2$  phase shift. The average retrieval accuracies in (d) and (e) are 98.9% and 96.0%, respectively.

realized in the spectral domain using the fast Fourier transform and the sign function.<sup>28</sup> The full field of the interferogram  $E_i(\phi)/E_r(\phi)$  is thus derived, from which the full signal field can be easily calculated by  $E_s(\phi) \approx |E_r(\phi)|(E_i(\phi)/E_r(\phi) - 1)$ . Here, we omit the negligible phase nonuniformity of the experimental reference beam. The retrieved signal field is then down-sampled, whose normalized amplitude  $|E_s(\phi)|$  and phase  $\arg(E_s(\phi))$  are plotted in the bottom panel of Fig. 2(b). Finally, the complex signal OAM spectrum is retrieved by taking the Fourier transform of  $E_s(\phi)$ . The step-by-step workflow for KK retrieval is described in Note S4 in the [Supplemental Material](#), and the code is also provided therein. Figure 2(c) shows the retrieved amplitude (top) and phase (bottom) profile of the OAM spectrum compared to the ground truth. It can be seen that they are in excellent agreement. To quantitatively assess the performance of the KK retrieval, we introduce the following metric based on the overlap integral of the target and the retrieved OAM spectra,

$$\eta = \frac{\left| \sum_{-\infty}^{\infty} a_l a'_l e^{i\theta_l - i\theta'_l} \right|^2}{\left( \sum_{-\infty}^{\infty} |a_l|^2 \right) \left( \sum_{-\infty}^{\infty} |a'_l|^2 \right)}, \quad (6)$$

where  $a'_l$  and  $\theta'_l$  are the amplitude and phase of the  $l$ th order OAM mode of the retrieved OAM spectrum, respectively. In Fig. 2(c), the retrieval accuracy  $\eta$  is found to be 97.6%.

To further test the validity of the proposed method, we apply the KK retrieval to diagnose a series of OAM spectra shown in Figs. 2(d) and 2(e). The first scenario is the rectangular OAM spectra  $E_s(\phi) = \sum_{l=1}^n e^{il\phi}$  of different widths ( $n = 1, 2, \dots, 20$ ), where the constituent OAM modes are of equal amplitudes and in-phase relations. Figure 2(d) shows the real and imaginary parts of the measured OAM spectra for these cases in a complex two-dimensional (2D) bar chart. As expected, the retrieved OAM spectra are approximately of rectangular shapes and are mainly populated in the real part of the bar chart due to their in-phase features. An average accuracy of 98.9% is achieved for these measurements. For the second scenario, the OAM spectra are structured by  $E_s(\phi) = e^{in\phi} + ie^{i(21-n)\phi}$ , where  $n = 1, 2, \dots, 20$ . In this case, the bar chart should be diagonal in its real part but antidiagonal in its imaginary part. This is clearly observed in the measurements shown in Fig. 2(e), with an average retrieval accuracy reaching 96.0%.

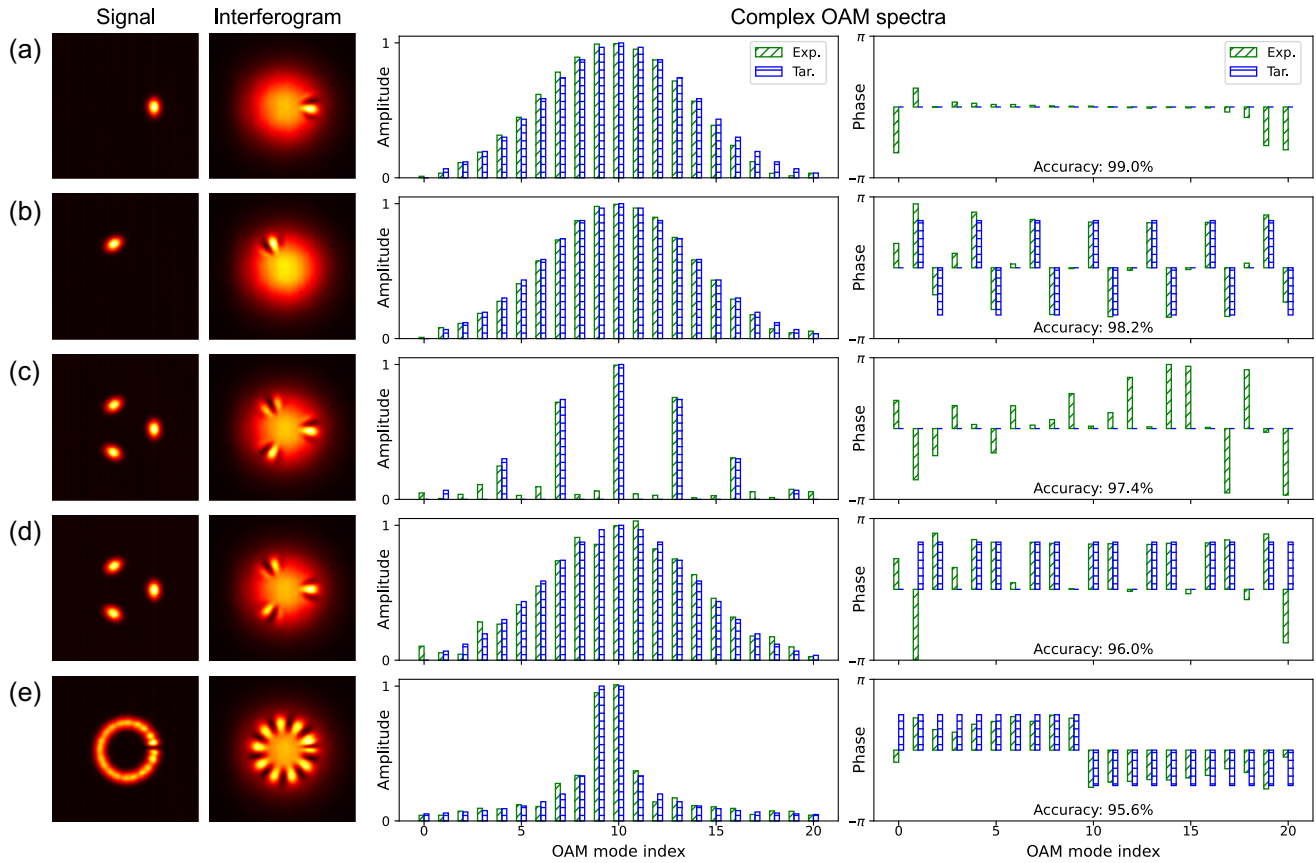


**Fig. 3** Measurements of complex OAM spectra. Left, the measured intensity images of the signal and the interferogram; right, the normalized amplitude and relative phase of the target and experimentally retrieved OAM spectrum. (a)–(d) Gaussian-shaped OAM spectra centered at 10th order with versatile OAM mode spacings and relative phase relations. (a) In-phase OAM spectrum with a mode spacing of 1. (b) Linear-phase OAM spectrum with a phase slope of  $2\pi/3$  and a mode spacing of 1. (c) In-phase OAM spectrum with a mode spacing of 3. (d) OAM spectrum with periodic Talbot phase  $[0, 2\pi/3, 2\pi/3]$  and a mode spacing of 1. (e) Fractional OAM mode with a topological charge of 9.5. The retrieval accuracy is also indicated for each case.

### 2.3 Measurement of Characteristic OAM States

The single-shot KK full-field retrieval allows for the simple characterization of complex OAM states. In the following, we study various characteristic OAM spectra displayed in Fig. 3. Figure 3(a) demonstrates the measurement of a signal field with a Gaussian-shaped, in-phase OAM spectrum centered at the 10th order, i.e.,  $E_s(\phi) = \sum_{l=1}^{20} e^{-\frac{(l-10)^2}{30}} e^{il\phi}$ , which corresponds to a bright petal horizontally aligned in the azimuthal angle.<sup>34</sup> From only a single interferogram, we can reconstruct the signal's OAM spectrum, which matches the ground truth well. As a single-shot retrieval method, we only use the interferograms to reconstruct the complex OAM fields. Note that all the measured images of the signal beams in Fig. 3 are displayed only as the ground truth and to help visualization of the signal fields, but they are not used for their OAM spectra retrieval. Figure 3(b) shows the condition for the same petal field as in Fig. 3(a) except being rotated by  $2\pi/3$  counterclockwise. A linear phase ramp is thus imparted to the OAM spectrum due to the rotation, with a phase slope of  $2\pi/3$ . This feature is well captured by the KK approach in a single-shot fashion, simplifying

the previously used schemes, such as the sequential weak and strong measurements<sup>35</sup> or the phase-shifting holograms.<sup>43</sup>

In addition, it is known that increasing the mode spacing in the OAM spectrum will lead to the multiplication of petals in the azimuthal angle.<sup>34</sup> This is shown in Fig. 3(c), where a three-petal field under test is constructed from in-phase OAM modes with an order spacing of 3 and the same envelope as in Figs. 3(a) and 3(b). The interferogram could accurately retrieve its equidistant OAM structure as well as its in-phase relation. Notice that the large phase error in Fig. 3(c) is only associated with void OAM modes or at small modal amplitudes. Furthermore, we investigate the complex OAM spectrum of the petal field in Fig. 3(c) being subjected to phase modulation. Specifically, when the three petals are modulated with the Talbot phase sequence of  $[0, -2\pi/3, -2\pi/3]$ , the initial OAM spectrum is self-imaged to create new OAM modes while preserving its overall envelope.<sup>37</sup> The measurement results are shown in Fig. 3(d). Although the signal intensity patterns in Figs. 3(c) and 3(d) are identical, the phenomenon of the OAM spectral self-imaging is clearly observed from the KK retrieval. More interestingly, the approach also provides a direct phase measurement of all

the OAM modes. It can be seen that the relative phases of OAM self-images again follow the Talbot relation of  $[0, 2\pi/3, 2\pi/3]$ , apart from a constant phase [subtracted thus not shown in Fig. 3(d) for better representability]. Notably, such a phase structure of Talbot self-images has only been recently determined in space<sup>44</sup> and time,<sup>45</sup> while here we measure it for the first time in the OAM basis. The measured quadratic phase relation suggests that the origin of self-imaging here is different from the Gouy-phase-mediated revivals of spatial fields.<sup>46–48</sup>

We also use the KK method to characterize the complex spectra of fractional OAM modes. A fractional OAM order can be viewed as the weighted superposition of integer OAM modes.<sup>49</sup> In Fig. 3(e), we show the measurement of the fractional OAM field with a topological charge of 9.5, i.e.,  $E_s(\phi) = e^{i9.5\phi}$ . The field intrinsically exhibits around 1% power leakage to the negative OAM orders, thus not rigorously satisfying the single-sideband requirement. Nevertheless, since the leakage is small, the KK retrieval still works effectively with an accuracy of 95.6%. We can see that the fractional OAM field in Fig. 3(e) is mainly composed of the 9th and 10th OAM modes, together with the other OAM orders slowly decaying when moving away from the center modes. Moreover, we are able to identify the phase relation of its constituent OAM modes, which is rarely explored for the fractional OAM states. It is found that the orders at the left and right parts of the fractional OAM spectrum are approximately out of phase. The phase deviation between the measured and theoretical fractional OAM spectra may come in part from the finite sampling in the azimuthal angle.

## 2.4 Effect of CSPR Levels

Figure 4 shows the KK retrieval performance at different CSPR levels. As an example, the same OAM state in Fig. 3(a) is used as the signal field for the study, whose complex amplitude field is displayed in Fig. 4(a). From this we can plot in Fig. 4(b) the trajectory of its azimuthal distribution in the complex plane. As mentioned previously, to guarantee rigorous KK retrieval, the trajectory of the signal field after interfering with the reference light must not encircle the origin of the complex plane. The minimum required reference intensity for such a criterion is highly dependent on the relative angle between the reference and the signal fields. In Fig. 4(b), the minimum required CSPR varies in a range between 5.1 and 11.3 dB, where the lower and upper bounds correspond to the reference field being added in-phase ( $\theta_r = 0$ ) and out-of-phase ( $\theta_r = \pi$ ) with the signal field, respectively. The minimum required CSPR value valid for all these relative angles is thus set by the upper bound, i.e., 11.3 dB.

Figure 4(c) presents the experimental results for the retrieval accuracy at different CSPR levels and various relative phases between the signal and reference fields. In the experiment, the control of the CSPR and its relative phase are realized via the computer-generated holograms. The phases shown in Fig. 4(c) are varied in steps of  $\pi/4$ . We emphasize here that they do not correspond to the actual  $\theta_r$ , but are offset from a constant unknown phase due to experimental constraints. In Fig. 4(c), when the experimental CSPR is well below the 11.3 dB threshold (marked by the dashed line), the retrieval performance changes significantly with the phase, although for some angles the retrieval accuracy is acceptable. Once the CSPR exceeds the threshold, decent retrieval is achieved for arbitrary relative phases between the reference and signal fields. The experimental

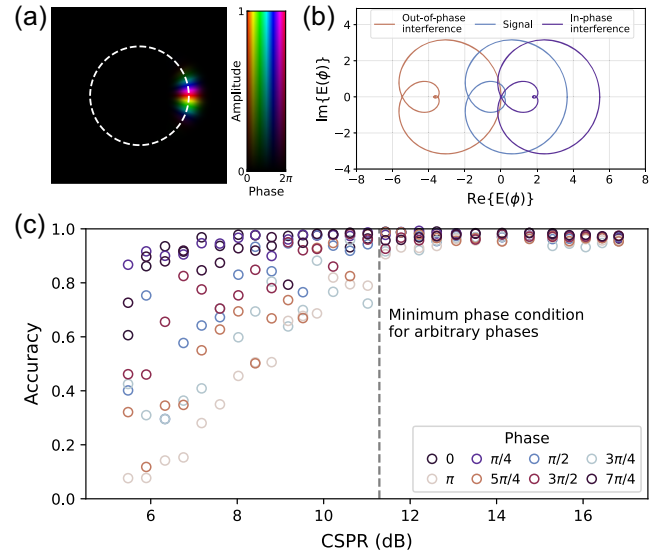


**Fig. 4** KK retrieval at different CSPR levels. (a) The complex amplitude field of the signal used for the study [the same as the signal field in Fig. 3(a)]. (b) The azimuthal trajectories of the signal field and interferograms with in-phase and out-of-phase addition of the reference field. The trajectories of interferograms are exactly at the limit of the minimum phase condition, which correspond to the minimum required CSPRs of 5.1 dB (in-phase) and 11.3 dB (out-of-phase), respectively. (c) The accuracy of the KK retrieval at different CSPR levels and varying phases between the signal and reference fields. Below the CSPR threshold for arbitrary phases (11.3 dB, indicated by the dashed line), the retrieval performance varies with the phase, while above, the retrieval accuracy is approximately close to the unity for all the phases.

results in Fig. 4(c) are in accordance with the theoretical analysis carried out above.

## 2.5 Performance Evaluation

In this part, we evaluate the performance of the KK retrieval on a large set of OAM spectra generated with random complex mode coefficients. As in the previous measurements, the difference between the experimental and minimum required CSPRs is automatically maintained around 1 dB, which is experimentally confirmed in Note S2 in the Supplemental Material for 100 random OAM spectra. Figure 5(a) shows the histogram of the KK retrieval accuracy for 1000 spectrum samples on the same dimensional space as before. An average retrieval accuracy of 95.6% is obtained, with a standard deviation of 1.2%. The performance of the KK retrieval is also compared with the conventional Fourier method,<sup>21,50</sup> computed by the Fourier transform disregarding the SSBI in Eq. (2). A clear advantage of using the KK method is shown in Fig. 5(a), suggesting that the SSBI cannot be neglected under such a CSPR level. Nevertheless, the field retrieved by the Fourier method does gradually approach the ground truth with the increase of CSPR values. The detailed discussion of the Fourier method can be found in Note S5 in the Supplemental Material. Next, we further push the measurement dimensionality up to the 30th OAM order while keeping the azimuthal sampling points and the digital upsampling unchanged. Figure 5(b) shows the



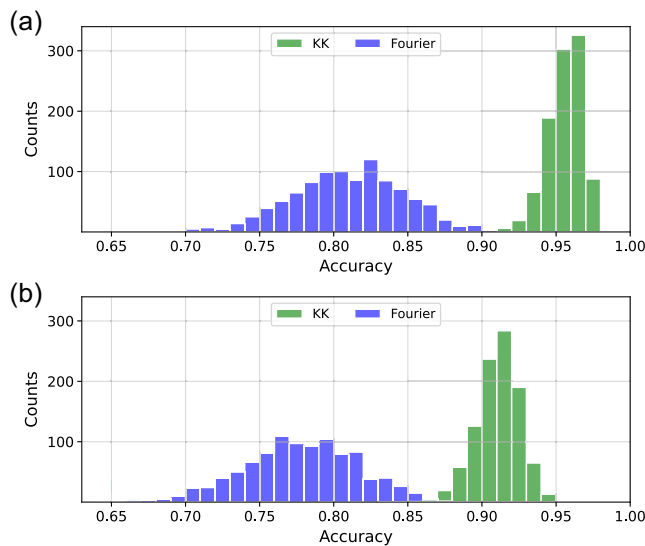


**Fig. 5** Performance evaluation of the KK retrieval on random OAM spectra. (a), (b) Histograms of the retrieval accuracy of the KK method and the conventional Fourier method, measured on 1000 OAM spectra with random complex mode coefficients. (a) For an OAM measurement range from 1 to 20, the average and standard deviation of the KK retrieval accuracy are 95.6% and 1.2%, respectively. (b) For an OAM measurement range from 1 to 30, the average and standard deviation of the KK retrieval accuracy are 91.1% and 1.4%, respectively. The KK method shows superiority over the Fourier method in both cases.

corresponding experimental results. The average KK retrieval accuracy in this case still reaches 91.1% with a standard deviation of 1.4%, outperforming the conventional Fourier method by a large margin. Although the performance of the Fourier method may be improved by increasing the reference power, keeping relatively low CSPR values is favored to avoid large DC components in detection, thus maximally utilizing the dynamic range of the camera.

### 3 Discussion

The experimental setup used in this work is a conventional on-axis interferometer equivalent to the configurations in Refs. 21–23. However, contrary to all the past demonstrations that require a few shots to diagnose a complex OAM spectrum, our method provides single-shot retrieval mediated by the famous KK relation. This greatly accelerates the measurement, as it bypasses the need to adjust the amplitude and/or phase of the reference when characterizing each superimposed state.<sup>21–23</sup> In our system, the speed of the measurement is defined by the frame rate of the camera. On the other hand, off-axis holography is also capable of retrieving full fields in a single shot and has been used to measure OAM beams.<sup>18</sup> While the conventional off-axis method requires separating SSBI and signals in the Fourier space, KK off-axis holography recovers the signal beam with a smaller off-axis angle.<sup>32</sup> In our work, the measurement is on-axis and thus different from KK off-axis holography. Further, the KK conditions in the off-axis method and our approach are also different, with the former in the wave vector space and the latter in the OAM space (see Note S6 in the [Supplemental Material](#)). To visualize the difference, we present in Note S6 in the

[Supplemental Material](#) an example that can be rigorously retrieved by our OAM KK method, using a reference beam whose wave vector component lies within the signal field in the wave vector space, while violating the condition for spatial KK retrieval. In addition, our approach demonstrates advantages when characterizing perfect vortex fields of narrow ring widths, as these beams take up a large space in the wave vector domain that requires high sampling resolution in off-axis holography. In addition, we discuss the choice of the sampling radius for retrieval in Note S7 in the [Supplemental Material](#). Recently, complex OAM spectrum analyzers have also been demonstrated using machine learning but require either dense layers of deep neural network<sup>51</sup> or a multitude of diffractive phase masks in cascade,<sup>52</sup> as well as being sensitive to the parameters of input fields, while our method can be easily extended to measuring multiple concentric OAM states as well as the superposition of Laguerre–Gaussian modes (see Note S8 in the [Supplemental Material](#)). Since in this study we are mainly dealing with only the azimuthal field distribution, the detection can be seamlessly connected to the rotational Doppler effect.<sup>53</sup> In this scenario, the camera is replaced by a fast photodetector with a spinning phase mask performing the azimuth-to-time mapping.<sup>21</sup>

To sum up this work, we propose and experimentally demonstrate a high-dimensional OAM analyzer that can measure complex OAM states in one single shot. The idea is inspired by the KK receiver in optical communications, while here we introduce the same concept to the OAM spectrum analysis and represent a new application scenario of KK phase retrieval. As demonstrated here, the proposed single-shot KK interferometry can be readily employed for state measurements in OAM-based information processing, sensing, and communication systems. This work also implies the general duality between azimuth-OAM and time-frequency, suggesting that their processing techniques may be borrowed interchangeably.

### Data, Materials, and Code Availability

Data underlying the results presented in this paper are not publicly available at this time but may be obtained from the authors upon reasonable request. A sample code for KK retrieval of OAM fields is provided at <https://github.com/GeorgeCravis/OAM-KK>.

### Acknowledgments

This work was supported by the National Key Research and Development Program of China (2018YFB1801803, 2019YFA0706302), the Basic and Applied Basic Research Foundation of Guangdong Province (2021B1515020093, 2021B1515120057), the Local Innovative and Research Teams Project of Guangdong Pearl River Talents Program (2017BT01X121), and the Swiss National Science Foundation (P2ELP2\_199825). The authors declare no conflicts of interest.

### References

1. D. Naidoo et al., “Controlled generation of higher-order Poincaré sphere beams from a laser,” *Nat. Photonics* **10**(5), 327–332 (2016).
2. A. Forbes, A. Dudley, and M. McLaren, “Creation and detection of optical modes with spatial light modulators,” *Adv. Opt. Photonics* **8**(2), 200–227 (2016).

3. A. E. Willner et al., “Optical communications using orbital angular momentum beams,” *Adv. Opt. Photonics* **7**(1), 66–106 (2015).
4. H. Rubinsztein-Dunlop et al., “Roadmap on structured light,” *J. Opt.* **19**(1), 013001 (2016).
5. M. J. Padgett, “Orbital angular momentum 25 years on,” *Opt. Express* **25**(10), 11265–11274 (2017).
6. M. Erhard et al., “Twisted photons: new quantum perspectives in high dimensions,” *Light Sci. Appl.* **7**(3), 17146 (2018).
7. Y. Shen et al., “Optical vortices 30 years on: OAM manipulation from topological charge to multiple singularities,” *Light Sci. Appl.* **8**(1), 90 (2019).
8. C. Schulze et al., “Measurement of the orbital angular momentum density of light by modal decomposition,” *New J. Phys.* **15**(7), 073025 (2013).
9. J. Hickmann et al., “Unveiling a truncated optical lattice associated with a triangular aperture using light’s orbital angular momentum,” *Phys. Rev. Lett.* **105**(5), 053904 (2010).
10. K. Dai et al., “Measuring OAM states of light beams with gradually-changing-period gratings,” *Opt. Lett.* **40**(4), 562–565 (2015).
11. S. Zheng and J. Wang, “Measuring orbital angular momentum (OAM) states of vortex beams with annular gratings,” *Sci. Rep.* **7**(1), 40781 (2017).
12. J. Leach et al., “Measuring the orbital angular momentum of a single photon,” *Phys. Rev. Lett.* **88**(25), 257901 (2002).
13. G. C. Berkhout et al., “Efficient sorting of orbital angular momentum states of light,” *Phys. Rev. Lett.* **105**(15), 153601 (2010).
14. M. P. Lavery et al., “Refractive elements for the measurement of the orbital angular momentum of a single photon,” *Opt. Express* **20**(3), 2110–2115 (2012).
15. M. Mirhosseini et al., “Efficient separation of the orbital angular momentum eigenstates of light,” *Nat. Commun.* **4**(1), 2741 (2013).
16. Y. Wen et al., “Spiral transformation for high-resolution and efficient sorting of optical vortex modes,” *Phys. Rev. Lett.* **120**(19), 193904 (2018).
17. G. Labroille et al., “Efficient and mode selective spatial mode multiplexer based on multi-plane light conversion,” *Opt. Express* **22**(13), 15599–15607 (2014).
18. N. K. Fontaine et al., “Laguerre-Gaussian mode sorter,” *Nat. Commun.* **10**(1), 1865 (2019).
19. Y. Zhang et al., “Simultaneous sorting of wavelengths and spatial modes using multi-plane light conversion,” arXiv:2010.04859 (2020).
20. H. Huang et al., “Phase-shift interference-based wavefront characterization for orbital angular momentum modes,” *Opt. Lett.* **38**(13), 2348–2350 (2013).
21. H.-L. Zhou et al., “Orbital angular momentum complex spectrum analyzer for vortex light based on the rotational Doppler effect,” *Light Sci. Appl.* **6**(4), e16251 (2017).
22. A. D’Errico et al., “Measuring the complex orbital angular momentum spectrum and spatial mode decomposition of structured light beams,” *Optica* **4**(11), 1350–1357 (2017).
23. S. Fu et al., “Universal orbital angular momentum spectrum analyzer for beams,” *PhotonIX* **1**(1), 19 (2020).
24. G. Kulkarni et al., “Single-shot measurement of the orbital-angular-momentum spectrum of light,” *Nat. Commun.* **8**(1), 1054 (2017).
25. E. Ip et al., “Coherent detection in optical fiber systems,” *Opt. Express* **16**(2), 753–791 (2008).
26. W.-R. Peng et al., “Spectrally efficient direct-detected OFDM transmission employing an iterative estimation and cancellation technique,” *Opt. Express* **17**(11), 9099–9111 (2009).
27. S. Randel et al., “100-Gb/s discrete-multitone transmission over 80-km SSMF using single-sideband modulation with novel interference-cancellation scheme,” in *Eur. Conf. Opt. Commun. (ECOC)*, IEEE, pp. 1–3 (2015).
28. A. Mecozzi, C. Antonelli, and M. Shtaif, “Kramers–Kronig coherent receiver,” *Optica* **3**(11), 1220–1227 (2016).
29. Z. Li et al., “SSBI mitigation and the Kramers–Kronig scheme in single-sideband direct-detection transmission with receiver-based electronic dispersion compensation,” *J. Lightwave Technol.* **35**(10), 1887–1893 (2017).
30. T. Bo and H. Kim, “Kramers–Kronig receiver operable without digital upsampling,” *Opt. Express* **26**(11), 13810–13818 (2018).
31. A. Mecozzi, C. Antonelli, and M. Shtaif, “Kramers–Kronig receivers,” *Adv. Opt. Photonics* **11**(3), 480–517 (2019).
32. Y. Baek et al., “Kramers–Kronig holographic imaging for high-space-bandwidth product,” *Optica* **6**(1), 45–51 (2019).
33. Y. Baek and Y. Park, “Intensity-based holographic imaging via space-domain Kramers–Kronig relations,” *Nat. Photonics* **15**(5), 354–360 (2021).
34. G. Xie et al., “Spatial light structuring using a combination of multiple orthogonal orbital angular momentum beams with complex coefficients,” *Opt. Lett.* **42**(5), 991–994 (2017).
35. M. Malik et al., “Direct measurement of a 27-dimensional orbital-angular-momentum state vector,” *Nat. Commun.* **5**(1), 3115 (2014).
36. J. Hu, C.-S. Brès, and C.-B. Huang, “Talbot effect on orbital angular momentum beams: azimuthal intensity repetition-rate multiplication,” *Opt. Lett.* **43**(16), 4033–4036 (2018).
37. Z. Lin et al., “Spectral self-imaging of optical orbital angular momentum modes,” *APL Photonics* **6**(11), 111302 (2021).
38. J. B. Götte et al., “Light beams with fractional orbital angular momentum and their vortex structure,” *Opt. Express* **16**(2), 993–1006 (2008).
39. P. Vaity and L. Rusch, “Perfect vortex beam: Fourier transformation of a Bessel beam,” *Opt. Lett.* **40**(4), 597–600 (2015).
40. A. Mecozzi, “A necessary and sufficient condition for minimum phase and implications for phase retrieval,” arXiv:1606.04861 (2016).
41. V. Cizek, “Discrete Hilbert transform,” *IEEE Trans. Audio Electroacoust.* **18**(4), 340–343 (1970).
42. V. Arrizón et al., “Pixelated phase computer holograms for the accurate encoding of scalar complex fields,” *J. Opt. Soc. Am. A* **24**(11), 3500–3507 (2007).
43. G. Xie et al., “Using a complex optical orbital-angular-momentum spectrum to measure object parameters,” *Opt. Lett.* **42**(21), 4482–4485 (2017).
44. H. G. De Chatellus et al., “Phases of Talbot patterns in angular self-imaging,” *J. Opt. Soc. Am. A* **32**(6), 1132–1139 (2015).
45. J. Clement, H. G. de Chatellus, and C. R. Fernández-Pousa, “Far-field Talbot waveforms generated by acousto-optic frequency shifting loops,” *Opt. Express* **28**(9), 12977–12997 (2020).
46. B. P. da Silva et al., “Pattern revivals from fractional Gouy phases in structured light,” *Phys. Rev. Lett.* **124**(3), 033902 (2020).
47. R.-Y. Zhong et al., “Gouy-phase-mediated propagation variations and revivals of transverse structure in vectorially structured light,” *Phys. Rev. A* **103**(5), 053520 (2021).
48. H.-J. Wu et al., “Conformal frequency conversion for arbitrary vectorial structured light,” *Optica* **9**(2), 187–196 (2022).
49. H. Zhang et al., “Review on fractional vortex beam,” *Nanophotonics* **11**(2), 241–273 (2022).
50. N. Bozinovic et al., “Control of orbital angular momentum of light with optical fibers,” *Opt. Lett.* **37**(13), 2451–2453 (2012).
51. H. Guo, X. Qiu, and L. Chen, “Simple-diffraction-based deep learning to reconstruct a high-dimensional orbital-angular-momentum spectrum via single-shot measurement,” *Phys. Rev. Appl.* **17**(5), 054019 (2022).
52. H. Wang et al., “Intelligent optoelectronic processor for orbital angular momentum spectrum measurement,” *PhotonIX* **4**(1), 9 (2023).
53. J. Courtial et al., “Measurement of the rotational frequency shift imparted to a rotating light beam possessing orbital angular momentum,” *Phys. Rev. Lett.* **80**(15), 3217–3219 (1998).



**Zhongzheng Lin** received his BS degree in physics from Dalian University of Technology, Dalian, China, in 2018. He is currently a PhD candidate in the School of Electronics and Information Technology at Sun Yat-sen University, Guangzhou, China. His research mainly focuses on the manipulation and detection of the structured light, especially optical vortices.

**Jianqi Hu** received his BE degree from the University of Electronic Science and Technology of China, in 2016, and his PhD in photonics from École Polytechnique Fédérale de Lausanne (EPFL), Switzerland, in 2021. He continued his research as a postdoc at EPFL from 2021 to 2022. Currently, he is an SNF postdoc fellow in Laboratoire Kastler Brossel, École Normale Supérieure, France. His research interests include integrated nonlinear photonics, frequency combs, orbital angular momentum, and optical computing.

**Yujie Chen** received his PhD in physics (photonics) from the Institute of Photonics, University of Strathclyde, Glasgow, United Kingdom, in 2012. He is currently a professor in the School of Electronics and Information Technology, Sun Yat-sen University, Guangzhou, China. His research interests include micro/nano-structured photonic devices for manipulating

light fields, as well as their applications in optical information processing and optical communications.

**Camille-Sophie Brès** received her bachelor's degree in electrical engineering from McGill University, Canada, in 2002, and her PhD in electrical engineering from Princeton University, USA, in 2007. After a postdoc at UCSD, she joined the Institute of Electrical Engineering at EPFL, Switzerland, where she is currently an associate professor. Her work focusses on leveraging and enhancing nonlinear processes in optical waveguides for the optimization of light conversion, signal processing, and sensing. She was elected fellow of Optica in 2019.

**Siyuan Yu** received his PhD in photonics from the University of Glasgow, United Kingdom, in 1997. He is currently a professor with Sun Yat-sen University, Guangzhou, China. He has helped in pioneering areas, such as high-speed integrated optical switches, microring lasers, integrated quantum photonics, and more recently, mode-division multiplexing devices and systems based on orbital angular momentum modes of light. He has published over 200 papers, including two cover features on science, and has been granted several international patents.